A&A 555, A108 (2013)
DOI: 10.1051/0004-6361/201321186

Astronomy & Astrophysics

Kepler observations of very low-mass stars

E. L. Martín[1,⋆], J. Cabrera[2], E. Martioli[3,4], E. Solano[5,6], and R. Tata[7]

[1] Centro de Astrobiología (INTA-CSIC), Carretera de Ajalvir km 4, 28550 Torrejón de Ardoz, Madrid, Spain
e-mail: ege@cab.inta-csic.es
[2] Institute of Planetary Research, German Aerospace Center, Rutherfordstrasse 2, 12489 Berlin, Germany
e-mail: Juan.Cabrera@dlr.de
[3] Canada-France-Hawaii Telescope, 65-1238 Mamalahoa Hwy, Kamuela, Hawaii 96743, USA
e-mail: eder@cfht.hawaii.edu
[4] Laboratório Nacional de Astrofísica (LNA/MCTI), Rua Estados Unidos, 154 Itajubá – MG, Brazil
e-mail: emartioli@lna.br
[5] Centro de Astrobiología (INTA-CSIC), Departamento de Astrofísica, PO Box 78, 28691 Villanueva de la Cañada, Madrid, Spain
e-mail: esm@cab.inta-csic.es
[6] Spanish Virtual Observatory
[7] Instituto de Astrofísica de Canarias, c/ Vía Láctea s/n, 28200 La Laguna, Tenerife, Spain
e-mail: rrtata@iac.es

Received 29 January 2013 / Accepted 9 May 2013

ABSTRACT

Observations of very low-mass stars with *Kepler* represent an excellent opportunity to search for planetary transits and to characterize optical photometric variability at the cool end of the stellar mass distribution. In this paper, we present low-resolution red optical spectra that allow us to identify 18 very low-mass stars that have *Kepler* light curves available in the public archive. Spectral types of these targets are found to lie in the range dM4.5–dM8.5, implying spectrophotometric distances from 17 pc to 80 pc. Limits to the presence of transiting planets are set by modeling of the *Kepler* light curves. We find that the size of the planets detectable by *Kepler* around these small stars typically lies in the range 1 to 5 Earth radii within the habitable regions ($P \leq 10$ days). We identify one candidate transit with a period of 1.26 days whose light curve resembles a planet slightly smaller than the Moon. However, our pixel by pixel analysis of the *Kepler* data shows that the signal most likely arises from a background contaminating eclipsing binary. For 11 of these objects reliable photometric periods shorter than 7 days are derived, and are interpreted as rotational modulation of magnetic cool spots. For 3 objects we find possible photometric periods longer than 50 days that require confirmation. The H_α emission measurements and flare rates are used as proxies for chromospheric activity, and transversal velocities are used as an indicator of dynamical ages. These data allow us to discuss the relationship between magnetic activity and detectability of planetary transits around very low-mass stars. We show that super-Earth planets with sizes around 2 Earth radii are detectable with *Kepler* around about two thirds of the stars in our sample, independently of their level of chromospheric activity.

Key words. astrobiology – techniques: photometric – techniques: spectroscopic – virtual observatory tools – stars: late-type – stars: flare

1. Introduction

Very low-mass (VLM) stars with spectral types between dM4 and dM7 constitute the most numerous population of the Milky Way (e.g., Lodieu et al. 2012, and references therein). Besides their ubiquity, they are interesting in their own right because of interesting physical processes that take place among them. The transition between partially and fully convective stellar interiors is expected to take place at spectral subclass dwarf (d) M3.5 (Cassisi 2011), and thus stars around this region are of considerable interest for studies of magnetic activity and rotation (Delfosse et al. 1998; Phan Bao et al. 2006). In this work we consider that the boundary between VLM stars and low-mass stars is located at spectral subclass dM4 (M4 dwarf).

The onset of metallic grain formation takes place at around spectral subclass dM7 (Jones & Tsuji 1997). Thus, dM7 objects and cooler are generically called ultracool dwarfs (UCDs). This term includes the L dwarfs (Martín et al. 1997) and cooler spectral types. Very late-M dwarfs and L dwarfs are known to display complex photometric variability that has been attributed to weather-like effects of the inhomogeneous distribution of dusty clouds in their photospheres (Martín et al. 2001; Bailer-Jones 2002). On the other hand, magnetic cool spots are thought to be the dominant source of surface inhomogeneities in VLM stars (Scholz & Eisloffel 2004).

The boundary between VLM stars and brown dwarfs (BDs) is located at M7 spectral subclass (Rebolo et al. 1995) in the Pleiades cluster. Most M dwarfs (dMs) in the general field are older than 100 Myr (Martín et al. 2010), so that late-M dwarfs in the *Kepler* field are likely to have stellar masses. Nevertheless, the lithium test has shown that it is possible to encounter some young BDs of very late-M spectral subclass even in the immediate solar vicinity (Tinney 1998; Martín et al. 1999b).

VLM stars have become attractive targets in the search for habitable rocky planets because their low masses and sizes favor the two most successful planet detection techniques, namely

⋆ Visiting Astronomer, Kitt Peak National Observatory, National Optical Astronomy Observatory, which is operated by the Association of Universities for Research in Astronomy (AURA) under cooperative agreement with the National Science Foundation.

high-precision radial velocity and transits, and renders transmission spectroscopy of Earth-sized planets in the habitable region around VLM stars potentially feasible with the future generation of large telescopes both in space and from the ground (Irwin et al. 2009; Kaltenegger & Traub 2009; Belu et al. 2011; Rauer et al. 2011; Pallé et al. 2011).

Radius measurements of a few VLM stars from angular diameter interferometric observations have recently become available (Lane et al. 2001). They have an accuracy below 10% and, combined with trigonometric parallaxes and photometry, have permitted determination of empirical relations to convert astronomical observables to astrophysical parameters that agree fairly well with theoretical models. The coolest single star with a direct size measurement is GJ 551 (dM5.5) for which a radius of 0.141 ± 0.007 *R*sun have been obtained (Demory et al. 2009). However, more accurate radii measurements using eclipsing binaries indicate that the theoretical models systematically underestimate the sizes of dM stars (Stassun et al. 2012).

VLM stars represent a challenge for the search of planets because of their high levels of magnetic activity (e.g., Goulding et al. 2012; Reiners et al. 2012), both from the point of view of transit searches and characterization (Tofflemire et al. 2012; Hartman et al. 2011; Berta et al. 2012; Law et al. 2012) as from the point of view of radial velocity surveys (e.g., Gomes da Silva et al. 2012). As a result, future surveys of planets around VLM primaries are strongly motivated, but their outcome may be optimized by appropriate selection of the best targets to minimize the effects of stellar activity.

Using a combination of different surveys, it has been estimated that in a sample of 100 dMs there could be one transiting habitable super-Earth (Rojas-Ayala et al. 2013). The *Kepler* NASA space mission provides a unique opportunity to study the time variability of dMs and to search for transiting planets around them. In this work we consider a sample of 18 VLM stars, which is too small to expect to detect one transiting planet, but it is nevertheless useful to estimate the sensitivity of *Kepler* to exoplanet transits at the low-mass tail of the stellar masses and to study the effects of magnetic activity on planet detectability.

The rest of this paper is organized as follows: Sect. 2 presents the selection criteria of the stars discussed in this paper. Section 3 deals with the spectroscopic observations of the sample. Section 4 discusses the analysis of *Kepler* light curves. Section 5 covers the derivation of stellar parameters for the sample. Finally, Sect. 6 provides our final remarks regarding future planet searches in VLM stars.

2. Target selection

Our VLM star candidates were selected using information obtained from the *Kepler* Input Catalog (KIC), the Two Micron All Sky Survey (2MASS, Skrutskie et al. 2006), and the Sloan Digital Sky Survey (SDSS, York et al. 2000). The following criteria were applied:

- $X_{\rm flg} = 0$ and $A_{\rm flg} = 0$, to avoid sources flagged in 2MASS as minor planets or contaminated by nearby extended sources;
- 2MASS $K_{\rm mag} > 9$, to eliminate red bright sources likely to be giants;
- $K_{\rm p} < 20$ (KIC photometry), to get rid of sources too close to the *Kepler* confusion limit.
- $r < 20$ (SDSS photometry), to keep sources bright enough for optical spectroscopic follow-up.
- $(r - J) > 4.0$ and $J - K < 1.05$ (2MASS and SDSS) to select red sources with colors similar to late-M dwarfs (West et al. 2011) but not so red in the infrared that there could be contamination by red giants (Bessell & Brett 1988).
- Total proper motions (PMs) obtained from the KIC larger than 0.1 arcsec/year.
- Light curves publicly available in at least two *Kepler* quarters.

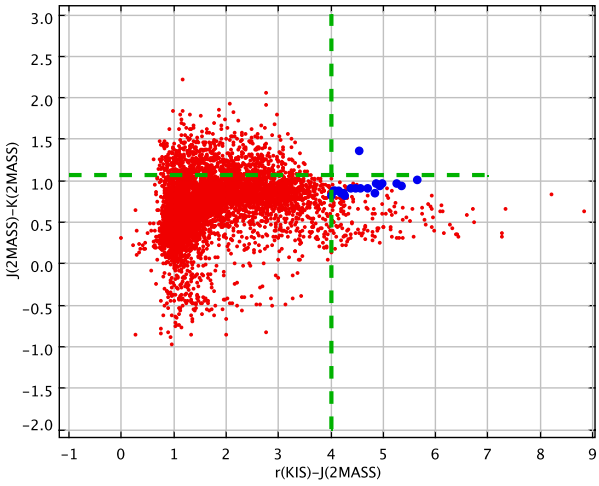

Fig. 1. Color–color diagram showing our KIC targets (blue) compared with a sample of 8000 KIC objects selected as described in the text but without color cuts. The only blue object outside the color-cut boundaries is the giant.

The color cuts are shown in Fig. 1 together with our VLM candidates and a subset of the stellar population in the *Kepler* field. Two additional KIC targets that do not meet all of the criteria given above were, nevertheless, included in our study; namely KIC 7435842, a photometric VLM star candidate without a PM value in the KIC, and KIC 8450707, a red giant candidate. As shown in the next section, our spectroscopic observations confirm KIC 7435842 as a VLM dwarf and KIC 8450707 as a red giant.

Astrometric and photometric data for the VLM candidates can be found in Table 1. Coordinates, *Kepler* passband magnitudes and proper motions were taken from the KIC. The *r*-band magnitudes were drawn from the SDSS, and near-infrared magnitudes were obtained from 2MASS.

Only one of our targets has been studied before, KIC 3330684, which is also named LSPM J1912+3826. It was identified as a star with annual proper motion higher than 0.15 arcsec (Lepine & Shara 2005). It is included in the stellar variability analysis of a sample of 129,000 dwarfs in the early data release of *Kepler* (Ciardi et al. 2011).

3. Spectroscopic follow-up

To assess the nature of VLM candidates, low-resolution red optical spectroscopy is well-known to be an effective method. Thus, follow-up spectroscopic observations of the targets were carried out using three different telescopes as follows:

- On 1 September 2011 and on 15–17 July 2012, the four-meter Mayall telescope at Kitt Peak National Observatory (KPNO) with the R.C./Cryocam spectrograph was used to obtain reconaissance spectra of the bulk of our VLM KIC candidates. The sky was patched with clouds, and often during the nights the dome had to be closed due to

Table 1. Astrometric and photometric data for our sample of VLM stars in the KIC.

KIC	RA(J2000) (hh:mm:ss.ss)	Dec(J2000) (dd:mm:ss.s)	r (SDSS)	Kp (KIC)	J (2MASS)	$J-K$ (2MASS)	PM (″/year)
6751111	18 45 25.95	42 14 53.2	17.35	16.58	13.26	0.87	0.101
7799941	18 45 43.65	43 31 08.5	19.52	19.53	13.86	1.00	0.116
11597669	18 55 25.53	49 37 52.1	16.72	16.03	12.70	0.81	0.118
8869922	19 00 05.65	45 07 06.1	16.03	16.05	11.89	0.87	0.134
3219046	19 06 10.79	38 19 36.8	17.65	17.66	13.45	0.83	0.120
4248433	19 09 37.68	39 23 26.0	15.72	15.74	11.33	0.89	0.132
3330684	19 12 28.09	38 26 15.8	15.90	15.92	11.20	0.89	0.330
5175854	19 13 30.91	40 22 26.9	18.30	18.32	13.83	0.90	0.174
7517730	19 14 21.48	43 09 00.8	17.22	17.23	12.38	0.84	0.186
7435842	19 15 59.81	43 05 41.6	17.94	17.95	13.00	0.92	
5353762	19 16 24.91	40 32 41.5	18.88	18.91	14.02	0.96	0.172
12108566	19 20 23.52	50 37 16.2	17.27	16.53	13.21	0.87	0.143
10538002	19 32 17.97	47 47 02.8	16.09	16.11	11.52	0.89	0.169
7691437	19 38 48.26	43 21 22.8	18.06	18.07	12.71	0.92	0.284
11356952	19 39 56.11	49 10 06.7	18.81	18.83	13.56	0.96	0.139
9033543	19 43 07.79	45 18 09.8	16.31	16.33	11.33	0.95	0.303
10285569	19 44 38.15	47 20 30.1	16.07	16.09	11.81	0.81	0.320
8450707	19 52 44.62	44 28 51.6	14.24	13.51	9.70	1.35	
6233711	19 56 21.93	41 31 48.2	16.59	16.59	12.35	0.83	0.124

Table 2. Spectroscopic log and results.

KIC	Date (UT)	Tel.	Texp (s)	Airmass	$EW(H_\alpha)$ (Å)	EW(NaI) (Å)	SpT
6751111	17 July 2012	KPNO	900	1.23	–5.9 ± 0.3	8.3 ± 0.2	dM4.5
7799941	2 Oct. 2011	NOT	1200	1.97	>–0.8	8.6 ± 0.6	dM7
11597669	17 July 2012	KPNO	360	1.60	–8.4 ± 0.9	8.8 ± 0.8	dM5
8869922	17 July 2012	KPNO	600	1.03	–10.1 ± 0.3	7.4 ± 0.3	dM5
3219046	16 July 2012	KPNO	600	1.01	–3.6 ± 0.4	7.8 ± 0.6	dM4.5
4248433	17 July 2012	KPNO	300	1.03	–6.9 ± 0.2	7.0 ± 0.2	dM5
3330684	15 July 2012	KPNO	600	1.28	–0.9 ± 0.2	7.4 ± 0.4	dM5
5175854	17 July 2012	KPNO	1200	1.41	–7.3 ± 0.3	8.7 ± 0.3	dM5
7517730	16 July 2012	KPNO	600	1.11	–1.2 ± 0.2	8.2 ± 0.2	dM6
7435842	15 July 2012	KPNO	1800	1.05	–1.8 ± 0.2	9.1 ± 0.2	dM6
5353762	10 July 2012	GTC	360	1.10	>–1.0	6.6 ± 0.3	dM6.5
12108566	17 July 2012	KPNO	600	1.28	–9.1 ± 0.4	7.7 ± 0.3	dM5
10538002	17 July 2012	KPNO	300	1.05	–4.5 ± 0.2	7.9 ± 0.3	dM5
7691437	1 Sept. 2011	KPNO	1800	1.58	–10.2 ± 0.3	10.6 ± 0.3	dM7.5
7691437	15 July 2012	KPNO	900	1.16	–8.4 ± 0.2	10.3 ± 0.2	dM7.5
11356952	2 Oct. 2011	NOT	900	1.74	–5.8 ± 0.5	8.3 ± 0.8	dM8.5
9033543	1 Sept. 2011	KPNO	600	1.03	>–0.7	7.8 ± 0.2	dM5.5
10285569	16 July 2012	KPNO	300	1.04	>–0.6	7.7 ± 0.5	dM4.5
8450707	15 July 2012	KPNO	300	1.08	>–0.8	3.4 ± 0.5	M4 III
6233711	17 July 2012	KPNO	900	1.06	–1.6 ± 0.2	7.2 ± 0.2	dM4.5
GJ 905	1 Sept. 2011	KPNO	120	1.04	–1.5 ± 0.2	7.9 ± 0.2	dM5 std.

thunderstorms. The BL181 grating and the 1.0 arcsec slit gave an effective resolution of 4.7 Å (*FWHM* = 1.69 pixels) as measured on emission lines. Order-sorting filters OG530 and GG475 were used to cut second-order light off in the 2011 and the 2012 runs, respectively. The spectra have an adequate signal-to-noise ratio S/N to be usable in the spectral range from 600 to 920 nm. The spectral type standard GJ905 was observed in 2011 for comparison purposes.

- On 2 October 2011, the 2.5-m Nordic Optical Telescope (NOT) with ALFOSC in the long slit observing mode was used to obtain spectra of KIC 7799941 and of KIC 11356952. The sky was clear and the seeing was below 1 arcsec. The grism number 5 and the 1.0 arcsec slit gave an effective resolution of 10.5 Å (*FWHM* = 2.24 pixels) as measured on emission lines. Order-sorting filter OG515 was used to cutoff second-order light.
- On 10 July 2012, the 10.4-m Gran Telescopio de Canarias (GTC) with OSIRIS in the long slit observing mode was used to obtain a spectrum of KIC 5353762. The sky was clear and the seeing was below 1 arcsec. The R500R grating and the 1.0 arcsec slit gave an effective resolution of 10.5 Å (*FWHM* = 2.24 pixels) as measured on emission lines.

All of the spectra were debiased, flatfielded, and extracted using the IRAF twodspec tools. Wavelength calibration was performed using arc lamps observed each night. The flux standard star EGGR39 was observed for calibration in each run, and it was used to correct for instrumental response and telluric contamination. Table 2 provides additional details for the observations of each target, as well as the main spectroscopic results, which are described next. Figure 2 displays all of our final spectra and shows the main spectral features used in the analysis.

Table 3. *Kepler* light curve results.

KIC	Np (points)	Baseline (days)	Period (days)	Flare number	Flare rate	Precision (5 σ) (%)	R_p/R_{Earth}
6751111	16 820	316.4	0.37,0.47	10	0.0023	2.0	2.6
7799941	16 820	316.4	53:	0	<0.0001	8.6	3.2
11597669	13 541	254.7	0.76	6	0.0022	2.7	2.7
8869922	16 820	316.4	0.70	14	0.0043	1.4	2.0(*)
3219046	16 820	316.4	0.49	4	0.0009	4.0	3.7
4248433	16 820	316.4	0.42	1	0.0002	9.5	5.4(*)
3330684	54 006	1016.0	51:	5	0.0005	0.2	0.8
5175854	16 820	316.4	0.56	0	<0.0001	4.7	3.8
7517730	16 820	316.4	62:	1	0.0002	0.7	1.2
7435842	16 820	316.4		0	<0.0001	1.3	1.6
5353762	16 820	316.4	33:	0	<0.0001	3.6	2.6
12108566	16 820	316.4	2.79	54	0.0154	3.2	3.1(*)
10538002	16 820	316.4	1.94	38	0.0102	0.8	1.6(*)
7691437	16 820	316.4	0.88	0	<0.0001	2.6	2.6(*)
11356952	16 820	316.4	0.16	19	0.0044	5.2	2.0
9033543	54 006	1016.0	50:	28	0.0020	0.3	0.9
10285569	12 445	234.1		0	<0.0001	0.3	1.0
8450707	476	9.0		0	<0.0001	–	–
6233711	16 820	316.4	6.53	3	0.0005	0.4	1.2

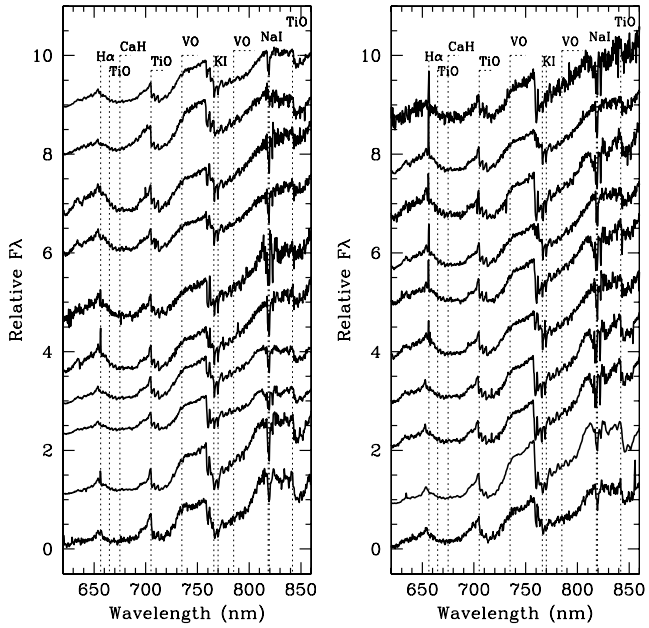

Fig. 2. Final spectra for our 18 confirmed KIC VLM dwarfs and one spectral-type reference star (GJ 905) and a giant (KIC 8450707). *Left panel*, from top to bottom the objects are GJ 905 (dM5), KIC 8450707 (M4III), KIC 6233711 (dM4.5), KIC 10285569 (dM4.5), KIC 3219046 (dM4.5), KIC 6751111 (dM4.5), KIC 3330684 (dM5), KIC 9033543 (dM5.5), KIC 7691437 (dM7.5) and KIC 11356952 (dM8.5). The main spectral features are labeled. *Right panel*, from top to bottom the objects are KIC 11597669 (dM5), KIC 8869922 (dM5), KIC 5175854 (dM5), KIC 4248433 (dM5), KIC 12108566 (dM5), KIC 10538002 (dM5), KIC 7517730 (dM6), KIC 7435842 (dM6), KIC 5353762 (dM6.5), KIC 7799941 (dM7).

3.1. Spectral typing and equivalent width measurements

The low-resolution spectra of VLM candidates were compared with reference spectra of late-M dwarfs coming from the literature (Henry et al. 1994; Martín et al. 1999a). Spectral types were derived by visual inspection of the closest spectral match. With these late-M spectral types the spectral regions around the VO bandhead at 730 nm and the TiO bandhead around 840 nm are particularly useful for classification, as is the steep pseudo-continuum slope between 760 and 810 nm.

Equivalent widths of H_α in emission, a chromospheric activity and mass accretion indicator (e.g., Barrado & Martín 2003) were measured by Gaussian fitting using the IRAF task splot. If no emission was seen, an upper limit was derived by direct integration of a 20 Å region centered on the wavelength of the H_α line (656.2 nm). None of the targets showed H_α emission that was strong enough to indicate active mass accretion.

Equivalent widths of the NaI subordinate doublet at 818 819 nm, which is an indicator of surface gravity in field late-M dwarfs (Martín et al. 2010), were measured by direct integration with splot. All the equivalent width measurements are given in Table 2. None of the targets were found to have any spectroscopic indication of extreme youth (age $\leq$ 100 Myr), such as NaI absorption equivalent width weaker than 6 Å, which is typical of Pleiades members of a similar spectral subclass (Steele & Jameson 1995). Thus, our spectroscopic results confirm the identification of 18 mature VLM stars in the *Kepler* public database.

4. *Kepler* light curves

All of the *Kepler* publicly released light curves for our targets have been utilized for this work. Most targets were observed in four quarters (Q6, Q7, Q8, and Q9) for GO20001 and GO20031. Two targets, namely KIC 3330684 and KIC 9033543, have been observed continuously since Q1. The baseline in days and number of usable light curve points for each target were computed from the FITS header keywords NAXIS2 and EXPOSURE and are summarized in Table 3. All of the targets were observed with the long cadence mode, so each point of the light curve corresponds to an exposure time of 30 min.

The light curves and the pixel mask data of our targets were downloaded by ftp from the *Kepler* mission archive at MAST in FITS format. These data files were used to search for transits and to determine periodicities and flare duty cycles, as described below.

4.1. Planet transit search

We used the algorithm DST (Cabrera et al. 2012) to search for transiting planets in the *Kepler* light curves of our targets. The algorithm proceeds in two steps; first it removes the long-term stellar variability with a Savitzky-Golay algorithm and the periodic stellar variability with a harmonic filter at the frequencies found by a Lomb-Scargle analysis of the data. The second step searches for the periodic signature of transiting planets. We have not found the signature of any reliable planetary transiting signal, although we have found transit-like features in the light curves of 3330684, 7517730, and 9033543, which are discussed below.

For this study, we have established two types of constraints, the first one based on the expected performance of transit detection algorithms and the second one, more conservative, based on the analysis of the scatter of the filtered light curves. The first constraint follows the procedure used by Howard et al. (2012). Assuming that the performance of transit detection algorithms evolves as expected for photometric surveys (Pont et al. 2006), and considering the detection performance of *Kepler* (Batalha et al. 2012) one can estimate the minimum planetary size detectable in our sample at a given stellar magnitude. Twelve out of the 18 dwarfs considered in this study have *Kepler* magnitudes brighter than 17.5, and extrapolating the performance of *Kepler*, we expect to be able to detect transit signals around these stars with depths of 500 ppm, or greater. For a star of 0.15 solar radii, this means a planet of the size of 0.37 Earth radii (only 30% larger than the Moon), which would be a breakthrough for transiting planets. Kepler-42d has a size of 0.57 Earth radii, the size of Mars (Muirhead et al. 2012).

Transit detection algorithms detect regularly periodic signals with amplitudes below the 1σ photometric scatter, which are undetectable by ocular inspection of individual transits. We have chosen, however, to set more conservative planet detections limits because we are aware that the stellar activity filtering and transit detection tools used in our study were optimized for solar-like stars. The stars in our sample show very irregular activity patterns, in particular flares and variable rotational modulation (in terms of amplitude and phase), which are challenging to filter out. Therefore, we have used a second constraint, much more conservative, in the same way as done for the search of transits for planets detected by radial velocity (Wang et al. 2012).

The principle of our conservative approach is to study the scatter of the light curve to rule out single transit features with a certain confidence level. The main difficulty is that transits of planets around VLM dwarfs typically last less than one hour, which is comparable to the *Kepler* long cadence integration time, and this means that single transit events might be represented by very few measurements (2–3). If the residuals were normally distributed, an event that deviates 5σ from the mean would only be produced once in every 1.74 million events. Typically, we have around 16 000 measurements per light curve (Table 3), so one would expect a very low impact from such outliers (typically, <1 case in 100 light curves). However, we must be aware that the outliers may not be normally distributed and that there could be residual instrumental effects in the data, which can mimic a transit (see discussion below). Therefore, for our conservative approach, we have tried to only rule out periodic transits, not single events.

We have chosen periods comparable to the expected position of the habitable zone of the host star ($P \leq 10$ days; Kaltenegger & Traub 2009) and ruled out transits with a depth of five times the scatter (5σ) by inserting transits of artificial planets in the light curves. We checked that the DST algorithm was able to detect all of the simulated transits down to the sensitivity limits provided in Table 3, where we give the 5σ scatter of the filtered light curve (our photometric precision) and the radius of the planet ruled out by our study in Earth units. For active stars (those denoted with asterisks in the eighth column of Table 3), we adopted a 10σ precision limit to estimate the radii of the planets. Typical values of planets detectable with DST in this sample range from one to five Earth radii. The dependence of the detectability of planet sizes with respect to *Kepler* magnitude is shown in Fig. 3. The planet size detectability does not depend linearly on target brightness because fainter stars tend to be cooler and have smaller radii than larger stars, and this compensates for their faintness.

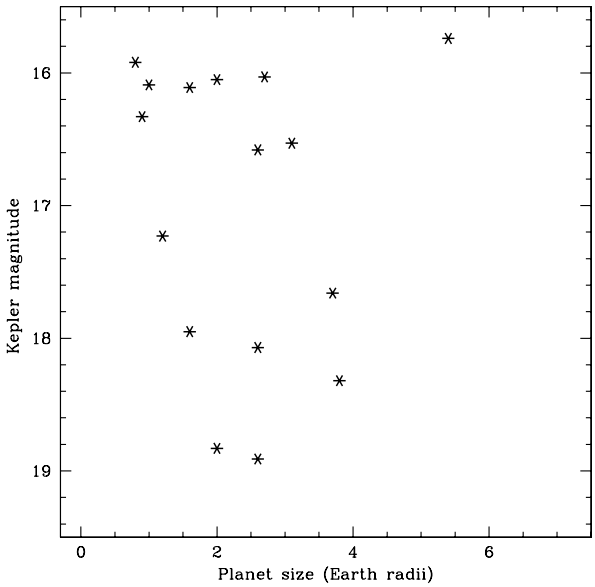

Fig. 3. Detectability of planets of different sizes with respect to *Kepler* magnitude in our sample of VLM stars. *Kepler* magnitudes are listed in Table 1. Planet sizes are given in units of Earth radii and are listed in Table 3.

4.1.1. The case of KIC 3330684

As an example of the short-period transit signals that can be detected by *Kepler* in VLM stars, we focus on KIC 3330684. When applied to the whole public *Kepler* data set consisting of 13 quarters (about 1141 days), DST shows the presence of a periodic transit-like signal with a period of 1.2613198 ± 0.0000016 days, an epoch $2\,451\,677.43109 \pm 0.00095$ in Julian Date, a depth of 190 ± 11 ppm, and a duration of 1.4 ± 0.1 h (Fig. 4). The detection of this signal is compatible with the detection limit expected from the candidate distribution reported by the *Kepler* team (Batalha et al. 2012), and it would correspond to an object of 0.24 Earth radii or 0.9 times the radius of the Moon, for a central transit and considering the radius of the dM5 host. However, the expected duration for a central transit around a dM5 star with this orbital period, and considering a circular orbit, is only 45 min, which is incompatible with the ephemeris found for the periodic signal. An eccentric orbit could account for a longer transit duration (see, for example, the case of Gliese 876 d, Rivera et al. 2010), but the simplest explanation is the presence of a contaminating eclipsing binary (CEB).

We have searched for the CEB responsible for the periodic signal using the centroid motion of the light curve and the information of the individual pixels of the *Kepler* mask (Fig. 5),

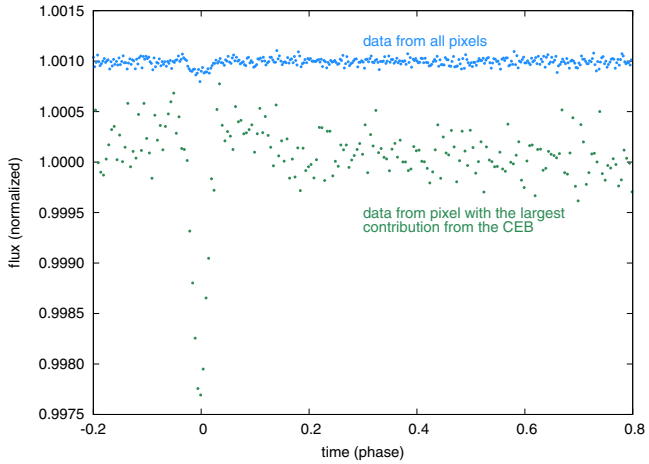

Fig. 4. Periodic transit-like signal in the light curve of KIC 3330684 folded with a period of 1.2613198 ± 0.0000016 days. Our pixel-by-pixel analysis indicates that the signal comes from an unidentified CEB located to the SW of the target.

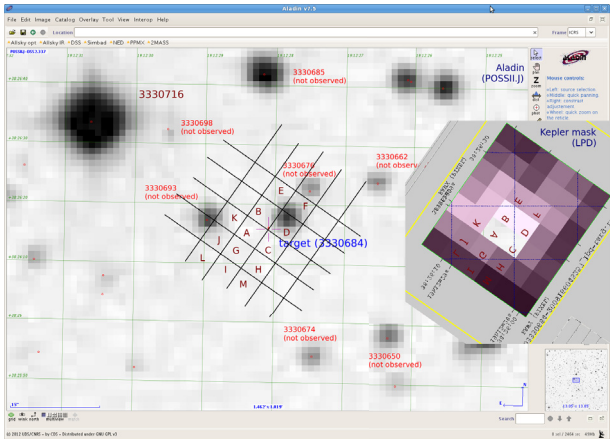

Fig. 5. Digital Sky Survey image of the field around KIC 3330684 with the *Kepler* pixel mask superimposed. The *Kepler* pixels analyzed in our study are labeled with capital letters.

following the approach of the *Kepler* team (Batalha et al. 2010). Their method is to analyze the centroid motion and study the behavior of the individual pixels of the *Kepler* mask. However, the information obtained during a single quarter is not enough to prove the presence of a CEB because the S/N is extremely low. By studying the position of the *Kepler* pixels in the sky, we combined the light of the pixels corresponding to the same region of the sky as observed in the different quarters. We have found that the ~200 ppm (0.02%) signal found by DST originates somewhere to the SE of the main target and has a depth about ten times larger (0.2%) and the clear V-shape of the grazing eclipse of a stellar binary (Fig. 4). We conclude that the origin of the periodic signal is not on target, although we have not been able to unambiguously identify the nature of the CEB, based on the available dataset. We have not found any source at the location of the CEB in the KIS catalog down to a magnitude limit of 21.5 in the IPHAS r-band (Greiss et al. 2012). However, this limit may not be sensitive enough. To produce the observed dips of 0.02% depth, the CEB can be up to 9.2 mag fainter than KIC 3330684. Given that the KIS r-band magnitude of KIC 3330684 is 15.82, deep imaging down to a sensitivity of 25th mag. in the optical is required to identify the CEB.

This example shows that we are able to detect extremely shallow short-period signals in the *Kepler* light curves of a VLM star. Finally, we note that KIC 3330684 is neither in the list of planetary candidates, nor in the list of false alarms of *Kepler* objects of interest (Batalha et al. 2012), however it is cited as a *Kepler* threshold crossing event by Tenenbaum et al. (2012).

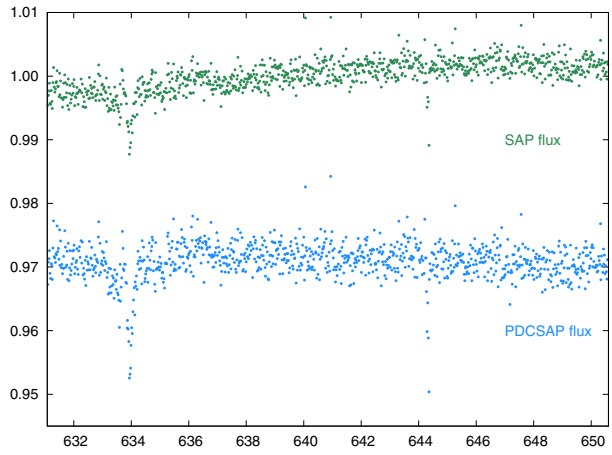

Fig. 6. Transit-like signals in the light curve of KIC 7517730, which are most likely due to instrumental effects as discussed in the text.

4.1.2. KIC 7517730 and KIC 9033543

As an example of instrumental residuals that can mimic transit-like events, we mention the examples of KIC 7517730 and KIC 9033543. KIC 7517730 shows two events with depths of around 1% and 2% (corresponding to planetary sizes, for central transits, of 1.4 and 2 Earth radii, respectively) as illustrated in Fig. 6. However, the shape of those events is similar to the pattern produced by instrumental effects identified in *Kepler* data, such as temperature fluctuations of the instrument or perturbations produced by solar particles (see Christiansen et al. 2012). When comparing the *Kepler* single-aperture photometry (SAP) and the pre-search data-conditioning photometry (PDCSAP), one can see how the PDCSAP correction enhances these features, which is a sign of their non astrophysical origin. SAP is the flux in units of electrons per second contained in the optimal aperture pixels collected by the spacecraft. PDCSAP is the flux contained in the optimal aperture in electrons per second after the PDC (pre-search data conditioning) module has applied its detrending algorithm to the PA (photometric analysis module) light curve. The *Kepler* data files are described in the document "*Kepler* archive manual" KDMC-10008-004 (`http://keplergo.arc.nasa.gov/Documentation.shtml`).

KIC 9033543 shows an odd pattern that we have not been able to find in the available documentation. It mimics the transit of a multiple system, making it extremely interesting, because multiple systems are thought to be bona-fide planetary systems (Lissauer et al. 2012). However, in this case the shape and the depth of the events depend on the correction applied to the data, therefore is indicative of an instrumental origin (Fig. 7).

These two examples illustrate the difficulty of characterizing the astrophysical origin of single transit events, which advocates for the use of the conservative constraints adopted in this paper.

4.2. Stellar variability

4.2.1. Rotational periods

Rotational periods were determined as a byproduct of the planetary transit search described above. As an independent check, the

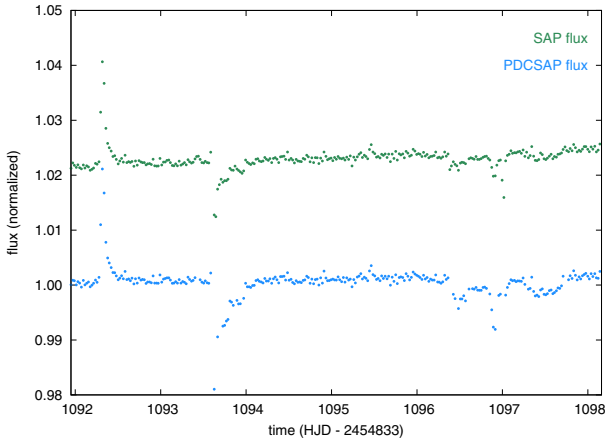

Fig. 7. Transit-like signals in the light curve of KIC 9033543, which are likely instrumental effects, as discussed in the text.

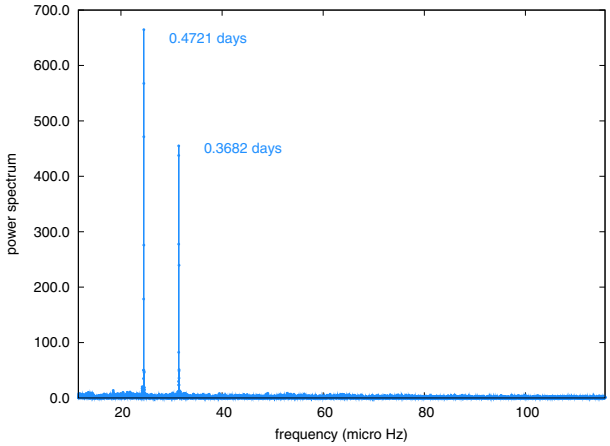

Fig. 8. Lomb-Scargle periodogram of KIC 6751111 (dM4.5). Two persistent periodicities are present in the data.

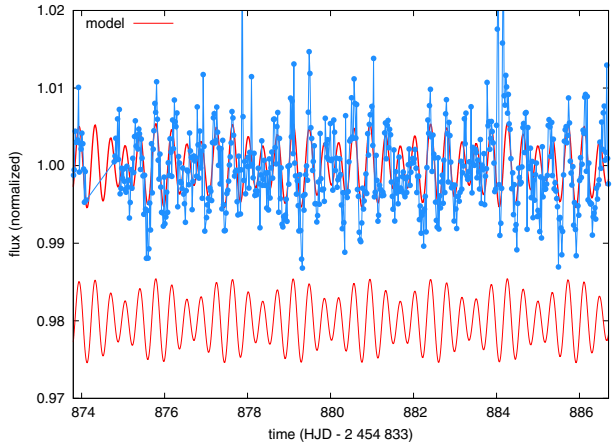

Fig. 9. Filtered *Kepler* light curve in Quarter 9 (upper line with dots) for KIC 6751111 compared with our model using the two periodicities found in the periodogram (lower curve). The model light curve is also supeposed on the data to show the fit.

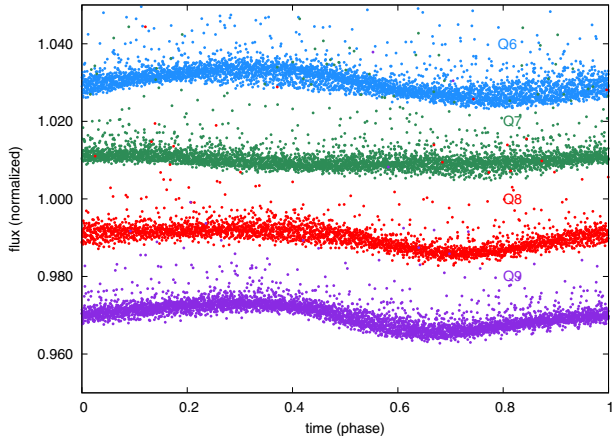

Fig. 10. *Kepler* light curves of KIC 8869922 folded with the same rotation period of 0.70 days in four different quarters (coded with different colors) to illustrate the evolution of surface features. The frequent upward excursions in flux are due to flares.

Kepler light curves of the targets were also fed into the NASA Star and Exoplanet Database (NStED) periodogram service. By default this service uses the Lomb-Scargle algorithm, but the box-fitting least squares and the Plavchan algorithms are also available. We used these three algorithms to check the robustness of the periods found by DST. Each quarter of data was analyzed independently. The periods provided in Table 3 were confirmed with two or more different algorithms. The periods marked with colons were not confirmed by two or more different algorithms, so they are considered as more uncertain. All of the confirmed periods have a low false-alarm probability (<0.01, as defined by Scargle 1982). We interpret all these periodicities as due to the rotational modulation of the light curves caused by spots in the atmospheres of the dwarfs.

KIC 6751111 is the only target in our sample that showed two persistent periodicities at 0.37 and 0.47 days (Fig. 8). This anomaly suggests that this object could be an unresolved binary composed of two components of similar brightness. It may be a member of the growing class of detached short-period M-dwarf binaries (Nefs et al. 2012). The *Kepler* light curve is well fitted by our algorithm using a combination of two sinusoidal curves with the periods derived from the periodogram (Fig. 9).

Ten targets have clear dominant periods shorter than seven days that we interpret as due to rotational modulation of long-lived surface features. The frequency of fast rotators in our sample ($v_{\rm rot} \geq 3$ km s^{-1} corresponding to Prot shorter than about 3 days) is 55%, which is in good agreement with previous estimates based on spectroscopic measurements of rotational broadening (Deshpande et al. 2012) that find about 65% of late dMs with $v \sin i$ higher than 12 km s^{-1}.

The high precision of *Kepler* allows us to obtain reliable rotational periods in 61% of the sample, a much higher detection rate than in ground-based transit surveys like MEarth, which reported rotation periods for 41 out of 273 (i.e., 15%) fully convective M dwarfs (Irwin et al. 2011), but comparable to the *Kepler*-based analysis for M dwarfs (McQuillan et al. 2013), which detected rotation periods in 63% of their sample (only one object in common with our sample).

The pattern of rotational variability often changes from one quarter to another, indicating that the surface features evolve with time. An example of this behavior is shown in Fig. 10. More data is needed to investigate the possible cyclic recurrence of these patterns.

The periods marked with colons in Table 3 are uncertain, and correspond to quiet VLM stars with possible rotation periods longer than 30 days. An example of our sinusoidal fit to the light curve of a slow rotator is given in Fig. 11. Such long periods are common among VLM stars (Irwin et al. 2011). Even longer photometric rotation periods (80–130 days) have been reported

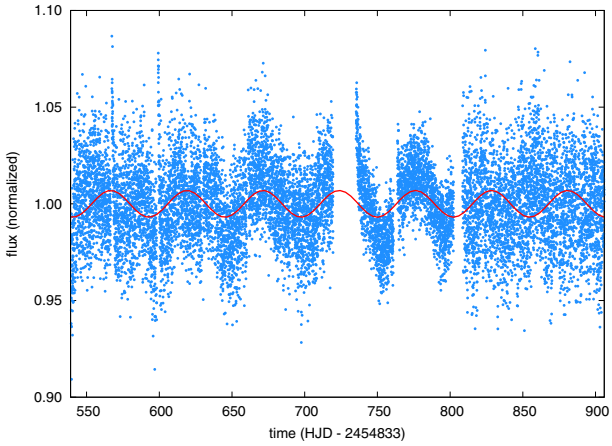

Fig. 11. The *Kepler* light curve (dots) of KIC 7799941 compared with our sinusoidal model (continuous line) with a rotation period of 53 days.

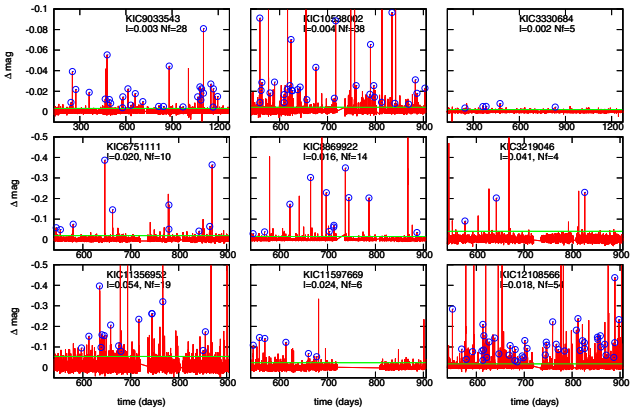

Fig. 12. A mosaic of our light curves showing more than three flares and the thresholds used to detect them (horizontal green lines). The number of flares (N_f) is given for each target.

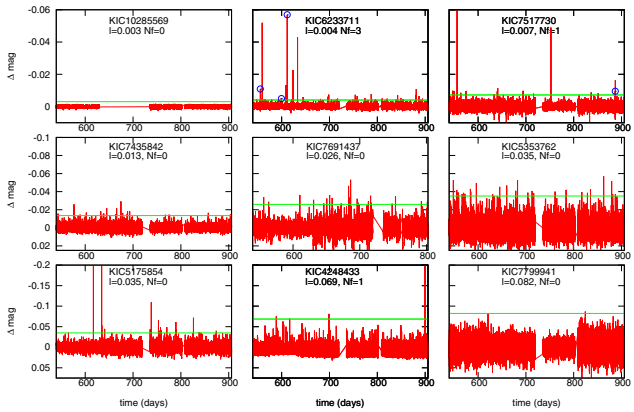

Fig. 13. A mosaic of our light curves showing fewer than three flares and the thresholds used to detect them (horizontal green lines). The number of flares (N_f) is given for each target.

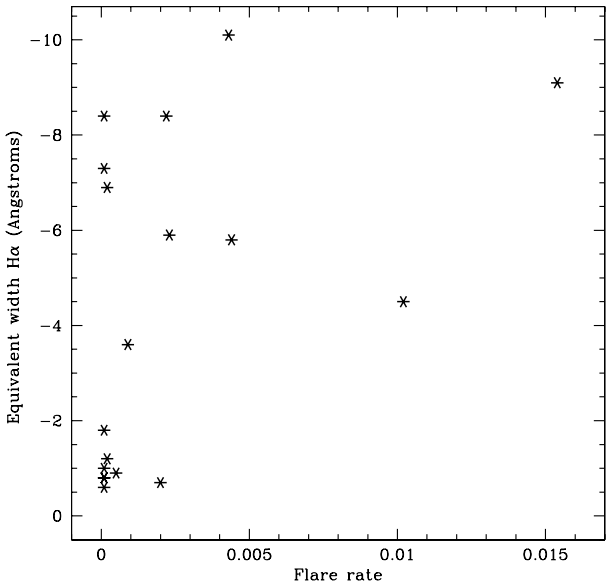

Fig. 14. H_α equivalent widths versus flare rates for our sample.

from Hubble Space Telescope monitoring of the very nearby VLM stars Proxima Centauri and Barnard's star (Benedict et al. 1998). However, we consider our long periods as tentative because we cannot rule out that they may arise from uncorrected long-term effects in the *Kepler* data.

4.2.2. Flares

We searched for flares using a custom-made algorithm to identify them. The algorithm proceeds in the following steps: (a) it calculates the median value of the light curve in two-day bins; (b) it calculates the median deviation; (c) it searches for upward flux excursions that are larger than a threshold (the threshold was set at a value equal to the median plus 5 times the median deviation); (d) it identifies flare events where the number of points above the threshold is larger than or equal to 3. This is a conservative criterion to eliminate high-frequency noise, intrumental glitches, or cosmic rays. The number of flares detected in each target are given in Col. 4 of Table 3. Figures 12 and 13 display the light curves and the thresholds used to detect the flares. Each detected flare is marked with a circle at the peak of the flux.

Very large flare events, where the peak flux surpassed in more than half a magnitude the quiescent brightness, were seen in KIC 8869922 (dM5), KIC 3219406 (dM4.5), KIC 4248433 (dM5), KIC 5175854 (dM5), KIC 12108566 (dM5), KIC 10538002 (dM5), and KIC 11356952 (dM8.5). The largest of them all was seen in KIC 12108566. It reached a nine times larger peak flux than the quiescent level and lasted several hours.

Flare rates were defined as the number of pixels were flares had been detected divided by the number of useful points in the light curve. The flare rates provided by us are probably lower limits in most cases because some short flares may have been missed by our conservative algorithm. A caveat of our method is that the flare rate we obtained depends on the noise characteristics of the light curves.

The rate of flares calculated for each target is given in Table 3, and Fig. 14 plots flare rates versus H_α equivalent widths. VLM stars with stronger H_α in emission have a higher incidence of flares, as expected because both phenomena are thought to be connected to the strength of magnetic fields. Three out of five VLM stars with H_α equivalent width $\leq$1 Å do not show any flare detection, and the other two have low flare rates.

5. Stellar parameters

So far, direct radius measurements obtained via ground-based interferometric observations have been available for only two

Table 4. Astrophysical parameters.

KIC	SpT	$T_{\rm eff}$ K	log g cm/s2	M/H	Radius $R/R_\odot$	A_v
6751111	dM4.5	3000 ± 50	5.0 ± 0.5	0.0 ± 0.5	0.17 ± 0.01	0.1 ± 0.1
7799941	dM7	2700 ± 300	5.5 ± 0.7	0.5 ± 0.5	0.10 ± 0.01	0.4 ± 0.1
11597669	dM5	3150 ± 50	5.0 ± 0.5	0.3 ± 0.5	0.15 ± 0.01	0.0
8869922	dM5	3100 ± 50	5.0 ± 0.5	0.3 ± 0.5	0.16 ± 0.01	0.1 ± 0.1
3219046	dM4.5	3000 ± 50	5.5 ± 0.5	–0.5 ± 0.5	0.17 ± 0.01	0.0
4248433	dM5	3000 ± 50	4.5 ± 0.5	0.0 ± 1.0	0.16 ± 0.01	0.0
3330684	dM5	2900 ± 50	4.5 ± 0.5	0.0 ± 0.5	0.16 ± 0.01	0.0
5175854	dM5	2700 ± 100	4.5 ± 0.5	0.5 ± 0.5	0.16 ± 0.01	0.1 ± 0.1
7517730	dM6	2800 ± 50	4.0 ± 0.5	0.0 ± 0.5	0.13 ± 0.01	0.1 ± 0.1
7435842	dM6	2700 ± 200	5.0 ± 1.0	0.5 ± 0.5	0.13 ± 0.01	0.0
5353762	dM6.5	2700 ± 200	4.5 ± 1.0	0.5 ± 0.5	0.12 ± 0.01	0.0
12108566	dM5	3000 ± 200	5.5 ± 0.5	0.3 ± 0.5	0.16 ± 0.01	0.1 ± 0.1
10538002	dM5	3000 ± 50	4.5 ± 0.5	0.0 ± 0.5	0.16 ± 0.01	0.0
7691437	dM7.5	2500 ± 150			0.10 ± 0.01	
11356952	dM8.5	2600 ± 300	5.0 ± 0.5	0.5 ± 0.5	0.08 ± 0.01	0.0
9033543	dM5.5	2900 ± 50	5.0 ± 0.5	0.3 ± 0.5	0.14 ± 0.01	0.2 ± 0.1
10285569	dM4.5	3150 ± 50	4.5 ± 0.5	-0.3 ± 0.5	0.17 ± 0.01	0.1 ± 0.1
8450707	M4 III	3350 ± 50	–0.5 ± 0.5	0.0		1.0 ± 0.1
6233711	dM4.5	3200 ± 50	5.0 ± 0.5	0.5 ± 0.5	0.17 ± 0.01	0.0

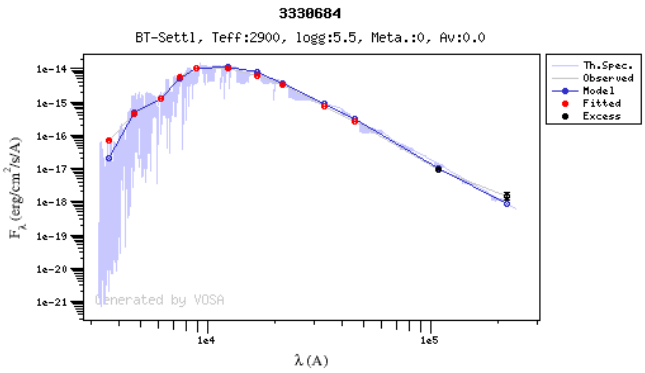

Fig. 15. VOSA SED fitting for one of our confirmed KIC VLM dwarfs (KIC 3330684, dM5). Catalog and synthetic photometric points are represented in red and blue, respectively. Points not considered in the fitting are shown in black. The best-fitting theoretical spectrum (from which the atmospheric parameters were derived) is also plotted.

VLM stars (e.g., Boyajian et al. 2012, and references therein), GJ 699 (dM4) and GJ 551 (dM5.5). A theoretical mass-spectral type relationship down to the substellar limit has been constructed by Baraffe & Chabrier (1996), but the luminosities that they used are not consistent with the interferometric data. For the sake of estimating the detectability of planetary transits in the *Kepler* light curves of our targets we used a linear relationship for the two VLM stars cited above and interpolated or extrapolated it using the spectral subclasses assigned to our targets. At spectral types later than dM7 we assume that the radius is constant due to electron degeneracy support. The results are provided in Table 4.

Effective temperatures ($T_{\rm eff}$) and surface gravities (log g) for our targets were obtained from χ^2 fitting of the spectral energy distribution (SED) using VOSA[1] (Virtual Observatory SED Analyzer, Bayo et al. 2008). Figure 15 provides an example of VOSA SED fitting. VOSA is a VO-tool designed to query several photometric catalogs accessible through VO services, as well as VO-compliant theoretical models, and it performs a statistical test to determine which model reproduces the observed data best. This approach has already been used to reveal new BDs in the WISE survey (Aberasturi et al. 2011). VOSA was able to distinguish the giant in our sample, and it generally provides $T_{\rm eff}$ that agree with our optically determined spectral types and a relation between $T_{\rm eff}$ and spectral subclass (Golimowski et al. 2004). The atmosphere models used by VOSA were the BT-Settl (Allard et al. 2012).

VOSA provided satisfactory fits for all our targets except for KIC 7691437. Archive images were inspected visually and it was found that KIC 7691437 WISE images are blended so that the VOSA results are not reliable. No blending with other objects was noticed for any of the other targets. For KIC 7691437, the $T_{\rm eff}$ was obtained directly from the spectral type (Golimowski et al. 2004).

5.1. Transversal velocities

Spectrophotometric distances for the confirmed VLM dwarfs were calculated using the 2MASS K-band magnitudes and a spectral type versus absolute K-band magnitude relation (Leggett et al. 2002). Transversal velocities were obtained from the total proper motion and the distance in parsecs. Results are provided in Table 5.

Transversal velocities have been used as a proxy for dynamical age in VLM stars (Zapatero Osorio et al. 2007). Those authors find that the mean transversal velocity of L and T dwarfs in the solar vicinity is lower than that of solar-type stars, and suggest that the UCDs could be kinematically younger, but a study of a larger sample that included late-M dwarfs did not reach the same conclusions (Faherty et al. 2009). We calculated equatorial rotational velocities for our targets using the rotational periods given in Table 3 and radii in Table 5. The rotational velocities are plotted versus the transversal velocities in Fig. 16. There seems to be a trend towards lower rotational velocity for higher transversal velocity as might be expected from evolutionary effects as the stars get older. This trend requires confirmation with a larger sample and with more accurate proper motion values

[1] http://svo.cab.inta-csic.es/theory/vosa/

Table 5. Spectrophotometric distances and transversal velocities of KIC VLM dwarfs.

KIC	SpT	K_{2MASS}	M_K	$m - M$ ±0.08	D pc	V_t km s^{-1}
6751111	dM4.5	12.39	8.18	4.21	69.5 ± 2.6	33.3 ± 1.2
7799941	dM7	12.86	9.90	2.96	39.1 ± 1.4	21.5 ± 0.8
11597669	dM5	11.89	8.41	3.48	49.7 ± 1.8	27.8 ± 1.0
8869922	dM5	11.02	8.41	2.61	33.3 ± 1.2	21.1 ± 0.7
3219046	dM4.5	12.62	8.18	4.44	77.3 ± 2.8	44.0 ± 2.1
4248433	dM5	10.44	8.41	2.03	25.5 ± 0.9	15.9 ± 0.6
3330684	dM5	10.31	8.41	1.90	24.0 ± 0.9	37.5 ± 1.4
5175854	dM5	12.93	8.41	4.52	80.2 ± 3.0	66.1 ± 2.5
7517730	dM6	11.54	9.17	2.37	29.8 ± 1.1	26.3 ± 1.0
7435842	dM6	12.08	9.17	2.91	38.2 ± 1.4	
5353762	dM6.5	13.06	9.17	3.89	60.0 ± 2.2	48.9 ± 1.8
12108566	dM5	12.34	8.41	3.93	61.1 ± 2.3	41.4 ± 1.6
10538002	dM5	10.63	8.41	2.22	27.8 ± 1.0	22.3 ± 0.8
7691437	dM7.5	11.79	9.92	1.87	23.7 ± 0.9	31.9 ± 1.1
11356952	dM8.5	12.60	10.55	2.05	25.7 ± 0.9	16.9 ± 0.7
9033543	dM5.5	10.38	9.17	1.21	17.5 ± 0.6	25.1 ± 0.9
10285569	dM4.5	11.00	8.18	2.82	36.6 ± 1.3	55.5 ± 2.0
6233711	dM4.5	11.52	8.18	3.34	46.5 ± 1.7	27.5 ± 1.1

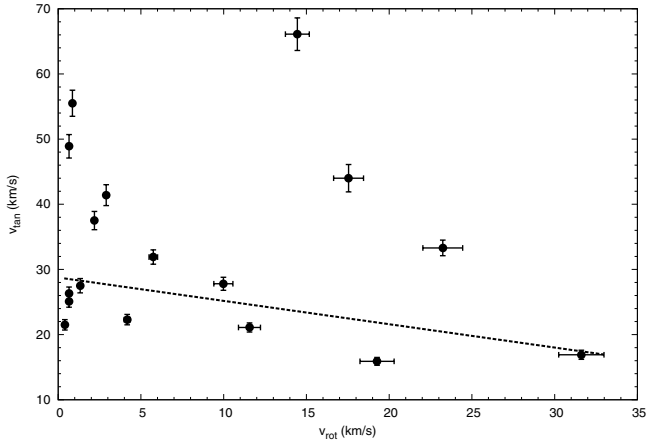

Fig. 16. Transversal velocities versus equatorial rotational velocities for 17 KIC VLM stars. A linear fit regression to the data is shown as a dotted line. All velocities are measured in units of km s^{-1}.

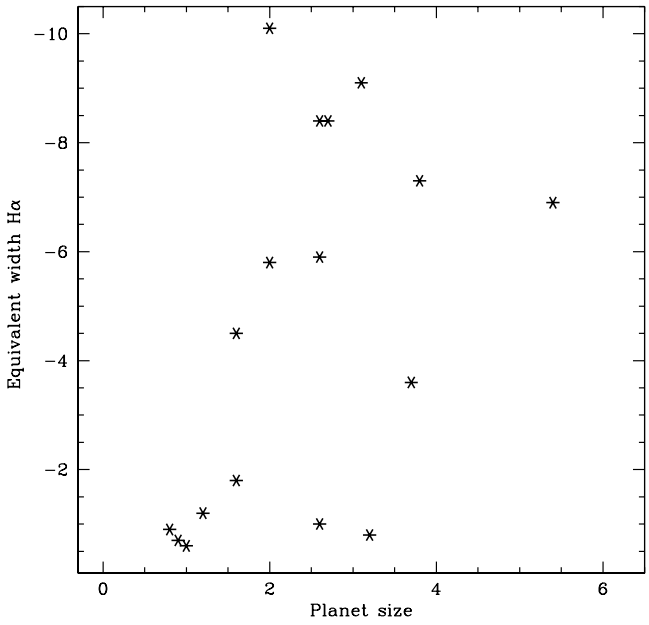

Fig. 17. H_α equivalent widths versus planet size detectability for our sample. Equivalent widths in Å, as listed in Table 2, and planet sizes in Earth radii, as listed in Table 3.

and radial velocity measurements for the VLM stars observed by *Kepler*.

6. Planet detectability

Planet detectability depends on the magnetic activity of the star, which is also related to the stellar rotation. Cool stars show higher levels of chromospheric activity for faster rotation and also higher jitter in radial velocity (Saar et al. 1998) and photometric flux variability (Lanza et al. 2011). Thus, planet detectability tends to be reduced in active cool stars, but it is not clear whether this trend continues into the ultracool dwarf domain.

In our sample, we checked the relation between H_α equivalent width as a proxy of chromosperic activity and planet size limits as a proxy to planet detectability. The results are shown in Fig. 17. Super-Earth planets with sizes around two Earth radii are detectable for any level of chromospheric activity. However, the detectability of the lowest planet sizes, around and even slightly below the radius of the Earth, is only reached for the quietest VLM stars. The result that the best sensitivity for planetary transits in VLM stars with *Kepler* is reached for the least chromospherically active VLM stars is tentative and needs to be tested with a larger sample.

Acknowledgements. This work is based (in part) on observations made with the Gran Telescopio Canarias (GTC), operated on the island of La Palma in the Spanish Observatorio del Roque de los Muchachos of the Instituto de Astrofísica de Canarias. This research has been supported by the Spanish Ministry of Economy and Competitiveness (MINECO) under grant AyA2011-30147-C03-03 and by the Consolider Ingenio 2010-GTC project. Part of the manuscript was written while EM was a visiting professor in the Geosciences Department at the University of Florida. The data presented here were obtained (in part) with ALFOSC, which is provided by the Instituto de Astrofísica de Andalucia (IAA) under a joint agreement with the University of Copenhagen and the NBIfAFG of the Astronomical Observatory of Copenhagen. This article is partly based on observations obtained with the Nordic Optical Telescope, jointly operated on the island of La Palma by Denmark, Finland, Iceland, Norway, and Sweden, in the Spanish Observatorio del Roque de los Muchachos of the Instituto de Astrofísica de Canarias. This publication makes use of data

products from the Two Micron All Sky Survey (2MASS), which is a joint project of the University of Massachusetts and the Infrared Processing and Analysis Center/California Institute of Technology, funded by the National Aeronautics and Space Administration and the National Science Foundation. Funding for the SDSS and SDSS-II has been provided by the Alfred P. Sloan Foundation, the Participating Institutions, the National Science Foundation, the US Department of Energy, the National Aeronautics and Space Administration, the Japanese Monbukagakusho, the Max Planck Society, and the Higher Education Funding Council for England. The SDSS Web Site is http://www.sdss.org/. The SDSS is managed by the Astrophysical Research Consortium for the Participating Institutions. The Participating Institutions are the American Museum of Natural History, Astrophysical Institute Potsdam, University of Basel, University of Cambridge, Case Western Reserve University, University of Chicago, Drexel University, Fermilab, the Institute for Advanced Study, the Japan Participation Group, Johns Hopkins University, the Joint Institute for Nuclear Astrophysics, the Kavli Institute for Particle Astrophysics and Cosmology, the Korean Scientist Group, the Chinese Academy of Sciences (LAMOST), Los Alamos National Laboratory, the Max-Planck-Institute for Astronomy (MPIA), the Max-Planck-Institute for Astrophysics (MPA), New Mexico State University, Ohio State University, University of Pittsburgh, University of Portsmouth, Princeton University, the US Naval Observatory, and the University of Washington. This research made use of the NASA Astrophysics Data System and of SIMBAD operated by the Centre de Donées Astronomiques de Strasbourg. IRAF is distributed by the National Optical Astronomy Observatory, which is operated by the Association of Universities for Research in Astronomy (AURA) under cooperative agreement with the National Science Foundation. Atmospheric parameters were estimated using VOSA, a VO-tool developed under the Spanish Virtual Observatory project supported from the Spanish MICINN through grant AyA2008-02156. The detailed referee report provided by Dr. Alex Scholz was useful to improve the original manuscript.

References

Aberasturi, M., Solano, E., & Martín, E. L. 2011, A&A, 534, L7
Allard, F., Homeier, D., Freytag, B., & Sharp, C. M. 2012, EAS, 57, 3
Bailer-Jones, C. A. L. 2002, A&A, 389, 963
Baraffe, I., & Chabrier, G. 1996, ApJ, 461, L51
Barrado y Navascués, D., & Martín, E. L. 2003, AJ, 126, 2997
Batalha, N. M., Rowe, J. F., et al. 2010, ApJ, 713, L103
Batalha, N. M., Rowe, J. F,. Bryson, S. T., et al. 2012, ApJS, 204, 24
Bayo, A., Rodrigo, C., Barrado y Navascués, D., et al. 2008, A&A, 492, 277
Belu, A. R., Selsis, F., Morales, J.-C., et al. 2011, A&A, 525, A83
Benedict, G. F., McArthur, B., Nelan, E., et al. 1998, AJ, 116, 429
Berta, Z. K., Irwin, J., Charbonneau, D., et al. 2012, AJ, 144, 145
Bessell, M. S., & Brett, J. M. 1988, PASP, 100, 1134
Boyajian, T. S., von Braun, K., van Belle, G., et al. 2012, ApJ, 757, 112
Cabrera, J., Csizmadia, S., Erikson, A., et al. 2012, A&A, 548, A44
Cassisi, S. 2011, MSAIt, in press
Christiansen, J. L., Van Cleve, J. E., Jenkins, J. M., et al. 2012, *Kepler* Data Characteristics Handbook (KSCI-19040-003)
Ciardi, D. R., von Braun, K., Bryden, G., et al. 2011, AJ, 141, 108
Delfosse, X., Forveille, T., Perrier, C., & Mayor, M. 1998, A&A, 331, 581
Demory, B.-O., Segransan, D., Forveille, T., et al. 2009, A&A, 505, 205
Deshpande, R., Martín, E. L., Montgomery, M. M., et al. 2012, AJ, 144, 99
Faherty, J. K., Burgasser, A. J., Cruz, K. L., et al. 2009, AJ, 137, 1
Golimowski, D. A., Leggett, S. K., Marley, M. S., et al. 2004, AJ, 127, 3516
Gomes da Silva, J., Santos, N. C., Bonfils, X., et al. 2012, A&A, 541, A9
Goulding, N. T., Barnes, J. R., Pinfield, D. J., et al. 2012, MNRAS, 427, 3358
Greiss, S., Steeghs, D., Gänsicke, B. T., et al. 2012, A&A, 144, 24
Jones, H. R. A., & Tsuji, T. 1997, ApJ, 480, L39
Hartman, J. D., Bakos, G. Á., Noyes, R. W., et al. 2011, AJ, 141, 166
Henry, T. J., Kirkpatrick, J. D., & Simons, D. A. 1994, AJ, 108, 1437
Howard, A. W., Marcy, G. W., Bryson, S. T., et al. 2012, ApJS, 201, 15
Irwin, J., Charbonneau, D., Nutzman, Ph., & Falco, E. 2009, Proc. IAU Symp., 253, 37
Irwin, J., Berta, Z. K., Burke, Ch. J., et al. 2011, ApJ, 727, 56
Kaltenegger, L., & Traub, W. A. 2009, ApJ, 698, 519
Lane, B. F., Boden, A. F., & Kulkarni, S. R. 2001, ApJ, 551, L81
Lanza, A. F., Boisse, I., Bonomo, A. S., & Moutou, C. 2011, A&A, 533, A44
Law, N. M., Kraus, A. L., Street, R., et al. 2012, ApJ, 757, 133
Leggett, S. K., Golimowski, D. A., Fan, X., et al. 2002, ApJ, 564, 452
Lepine, S., & Shara, M. M. 2005, AJ, 129, 1483
Lissauer, J. J., Marcy, G. W., Rowe, J. F., et al. 2012, ApJ, 750, 112
Lodieu, N., Espinoza Contreras, M., Zapatero Osorio, M. R., et al. 2012, A&A, 542, A105
Martín, E. L., Basri, G., Delfosse, X., & Forveille, T. 1997, A&A, 327, L29
Martín, E. L., Delfosse, X., Basri, G., et al. 1999a, AJ, 118, 2466
Martín, E. L., Basri, G., & Zapatero Osorio, M. R. 1999b, AJ, 118, 2466
Martín, E. L., Zapatero Osorio, M. R., & Lehto, H. J. 2001, ApJ, 557, 822
Martín, E. L., Phan Bao, N., Bessell, M., et al. 2010, A&A, 517, 53
McQuillan, A., Aigrain, S., & Mazeh, T. 2013, MNRAS, in press [arXiv:1303.6787]
Muirhead, P. S., Johnson, J. A., Apps, K., et al. 2012, ApJ, 747, 144
Nefs, S. V., Birkby, J. L., Snellen, I. A. G., et al. 2012, MNRAS, 425, 950
Pallé, E., Zapatero Osorio, M. R., & García Muñoz, A. 2011, ApJ, 728, 19
Phan Bao, N., Martín, E. L., Donati, J.-F., & Lim, J. 2006, ApJ, 646, L73
Pont, F., Zucker, S., & Queloz, D. 2006, MNRAS, 373, 231
Rauer, H., Gebauer, S., Paris, P. V., et al. 2011, A&A, 529, A8
Rebolo, R., Zapatero Osorio, M. R., & Martín, E. L. 1995, Nature, 377, 129
Reiners, A., Joshi, N., & Goldman, B. 2012, AJ, 143, 93
Rivera, E. J., Laughlin, G., Butler, R. P., et al. 2010, ApJ, 719, 890
Rojas-Ayala, B., Hilton, E. J., Mann, A. W., et al. 2013, Astron. Nachr., 334, 1
Saar, S. H., Butler, R. P., & Marcy, G. W. 1998, ApJ, 498, L153
Scargle, J. D. 1982, ApJ, 263, 835
Scholz, A., & Eisloffel, J. 2004, A&A, 421, 259
Skrutskie, M. F., Cutri, R. M., Stiening, R., et al. 2006, AJ, 131, 1163
Stassun, K. G., Kratter, K. M., Scholz, A., & Dupuy, T. J. 2012, ApJ, 756, 47
Steele, I. A., & Jameson, R. F. 1995, MNRAS, 272, 630
Tenenbaum, P., Jenkins, J. M., Seader, S., et al. 2012, ApJS, 199, 24
Tinney, C. G. 1998, MNRAS, 296, L42
Tofflemire, B. M., Wisniewski, J. P., Kowalski, A. F., et al. 2012, AJ, 143, 12
Wang, S. X., Wright, J. T., Cochran, W., et al. 2012, ApJ, 761, 46
West, A. A., Morgan, D. P., Bochansky, J. J., et al. 2011, AJ, 141, 97
York, D. G., Adelman, J., Anderson, J. E., et al. 2000, AJ, 120, 1579
Zapatero Osorio, M. R., Martín, E. L., Béjar, V. J. S., et al. 2007, ApJ, 666, 1205